Proceedings of the ASME 2010 3rd Joint US-European Fluids Engineering Summer Meeting and 8th International Conference on Nanochannels, Microchannels, and Minichannels
FEDSM-ICNMM2010
August 1-5, 2010, Montreal, Canada

FEDSM-ICNMM2010-30810

A THREE EQUATION CURVATURE AND ROTATION SENSITIVE VARIANT OF THE SST K-OMEGA TURBULENCE MODEL

Tej Prasad Dhakal and D. Keith Walters
CAVS SimCenter
Department of Mechanical Engineering
Mississippi State University
Mississippi State, MS 39762

ABSTRACT

To date, eddy viscosity models are the most accepted and widely used RANS-based turbulence closures, attributable to their computational efficiency and relative robustness. One notable shortcoming of these models is their insensitivity to system rotation and streamline curvature. In this article, we present a variation of the SST k-ω model properly sensitized to system rotation and streamline curvature. The new model is based on a direct simplification of the Reynolds Stress Model under weak equilibrium conditions. To enhance stability and include history effects, an additional transport equation for a transverse turbulent velocity scale is added to the model. The new transport equation incorporates the physical effect of curvature and rotation on the turbulence structure. The eddy viscosity is then redefined based on the new turbulent velocity scale. The model is calibrated based on rotating homogeneous shear flow and implemented for a number of test cases including rotating channel, U-duct, and hump model flow. Compared to popular two equation models, the new model shows improved performance in system rotation and/or streamline curvature dominated flows.

INTRODUCTION

Turbulent flows of engineering interest often have the effects of body forces induced by system rotation and curvature. Conventional eddy viscosity models (EVM) are not sensitized to these effects and thus fail to reproduce their effect in the flow. Although there are a number of Second Moment Closure (SMC) based algebraic stress models, and similarly non-linear eddy viscosity models (NLEVM), capable of resolving the rotation and curvature effects, their use is limited due to added computational cost and numerical stiffness. EVMs are still the most preferred turbulence closures in the industrial CFD community. In this paper, we present a variant of the SST k-ω model with one additional scalar transport equation, which is intended to capture the effects of system rotation and/or streamline curvature. The new transport equation is a compromise between robustness and computational efficiency. The new scalar variable scales with the transverse turbulent velocity and carries the turbulence structure information. The eddy viscosity is redefined using the new scaling argument in such a way that it embraces the effects of rotation and curvature (RC) on the turbulent flow, and yields results equivalent to the SST k- ω model when these effects are not significant. The imposed rotation rate or the rotational effect due to streamline curvature is included in the source term for the new scalar transport equation. The form of the proposed model is easily expandable to 3D flows. In the following sections, the turbulence model formulation and a number of test case results including rotating homogeneous shear, rotating turbulent channel flow, fully developed U-bend flow, and hump model flow are discussed.

MODEL FORMULATION

For purposes of modeling, the Reynolds stress tensor in incompressible flow may be expressed in terms of the turbulent kinetic energy, k, and the anisotropy tensor b_{ij} defined as:

$$b_{ij} \equiv \frac{\overline{u_i u_j}}{k} - \frac{2}{3}\delta_{ij} \,. \tag{1}$$

The anisotropy tensor contains the relevant information on turbulence structure and must be evaluated as a function of available variables in the simulation. Gatski and Speziale [1] proposed an explicit functional form for the anisotropy tensor

based on the weak equilibrium hypothesis, which forms the basis for their algebraic Reynolds stress model:

$$b_{ij} = \frac{\left(\frac{4}{3} - C_2\right)}{(C_3 - 2)} \cdot \frac{6}{3 - 2\eta^2 + 6\zeta^2} \cdot \left[S_{ij}^* + \left(S_{ik}^* W_{kj}^* + S_{jk}^* W_{ki}^* \right) - 2\left(S_{ik}^* S_{kj}^* - \frac{1}{3} S_{kl}^* S_{kl}^* \delta_{ij} \right) \right] \quad (2)$$

where

$$\eta^2 = S_{ij}^* S_{ij}^* \quad , \quad (3)$$

$$\zeta^2 = W_{ij}^* W_{ij}^* \quad , \quad (4)$$

$$S_{ij}^* = \frac{1}{2} g \frac{k}{\varepsilon} (2 - C_3) S_{ij} \quad , \quad (5)$$

$$W_{ij}^* = \frac{1}{2} g \frac{k}{\varepsilon} (2 - C_4) W_{ij} \quad , \quad (6)$$

$$W_{ij} = \Omega_{ij}^{'} + \frac{(C_4 - 4)}{(C_4 - 2)} e_{mji} \omega_m \quad , \quad (7)$$

$$g = \left(\frac{1}{2} C_1 + \frac{P^k}{\varepsilon} - 1 \right)^{-1} \quad . \quad (8)$$

Note that S_{ij} represents the rate-of-strain tensor and $\Omega_{ij}^{'}$ represents the rotation rate tensor expressed in a reference frame rotating with angular velocity ω_m:

$$S_{ij} = \frac{1}{2} \left(\frac{\partial U_i}{\partial x_j} + \frac{\partial U_j}{\partial x_i} \right) \quad , \quad (9)$$

$$\Omega_{ij}^{'} = \frac{1}{2} \left(\frac{\partial U_i}{\partial x_j} - \frac{\partial U_j}{\partial x_i} \right) \quad . \quad (10)$$

York et al. [2] linearized the explicit algebraic anisotropy tensor with respect to mean strain rate to develop a semi-implicit expression for eddy-viscosity coefficient and used it to redefine eddy viscosity and developed a curvature sensitive k-ε model:

$$C_\mu = \frac{K_1 + K_2 C_\mu \left(\frac{Sk}{\varepsilon} \right)^2 + K_3 C_\mu \left(\frac{Sk}{\varepsilon} \right) + K_4 C_\mu^2 \left(\frac{Sk}{\varepsilon} \right)^3}{K_5 + K_6 C_\mu \left(\frac{Sk}{\varepsilon} \right)^2 K_7 C_\mu^2 \left(\frac{Sk}{\varepsilon} \right)^4 + K_8 \left(\frac{Wk}{\varepsilon} \right)^2} \quad , \quad (11)$$

where S is the strain rate magnitude, K_1 – K_8 are model constants, and ε is turbulence dissipation rate. In adopting this expression for the SST k-ω model, the dissipation rate is expressed as $\varepsilon = 0.09 k\omega$. The effect of curvature and rotation is included in the term ω_m, and enters in the eddy-viscosity expression via the effective rotation rate magnitude term W:

$$W = \sqrt{2 W_{ij} W_{ij}} \quad . \quad (12)$$

Equation (7) can be alternately expressed:

$$W_{ij} = \Omega'_{ij} + e_{mji} \omega_m + \frac{-2}{C_4 - 2} e_{mji} \omega_m \quad , \quad (13)$$

$$W_{ij} = \Omega_{ij} + \frac{2}{C_4 - 2} \Omega_{ij}^r \quad , \quad (14)$$

where $\Omega_{ij} = \Omega_{ij}^{'} + e_{mji} \omega_m$ is the absolute vorticity tensor, expressed in an inertial frame of reference, and $\Omega_{ij}^r = -e_{mji} \omega_m$ is the coordinate system rotation rate tensor, also referred to as the vorticity modification tensor [3]. Although mathematically similar, the effect of a rotating reference frame modifies vorticity uniformly everywhere in the flow-field, whereas the influence due to curvature effects might change with both time and space throughout the domain.

In order to be frame indifferent and include the effects of rotation/curvature on the eddy viscosity, the term ω_m that appears in Eq. (11) is taken to be the local Lagrangian rotation rate of the principal axes of the mean strain rate tensor, similar to previous approaches in the literature [4-8]. In order to close the model, ω_m must be computed from the mean velocity field. In the present model formulation, we make use of Wallin and Johansson's [4] derivation for ω_m, which was also adopted by Spalart and Shur [8] and Gatski and Jongen [5] for curvature-corrected versions of the Spalart-Allmaras model and an algebraic Reynolds stress model, respectively:

$$\omega_i = A_{ij}^{-1} S_{pl} \dot{S}_{lq} e_{pqj} \quad (15)$$

where $\dot{S}$ is the material derivative of strain rate tensor and

$$A_{ij}^{-1} = \frac{II_s^2 \delta_{ij} + 12 III_s S_{ij} + 6 II_s S_{ik} S_{kj}}{2 II_s^3 - 12 III_s^2} \quad . \quad (16)$$

II_s and III_s are second and third invariants of the mean strain rate tensor. For 2D mean flows, equation (15) reduces to

$$\omega_3 = \frac{S_{11} \dot{S}_{12} - S_{12} \dot{S}_{11}}{2 S_{11}^2 + 2 S_{12}^2} \quad . \quad (17)$$

The transport equations used in the SST k- ω model are

$$\frac{\partial}{\partial t}(\rho k) + \frac{\partial}{\partial x_i}(\rho u_i k) = \frac{\partial}{\partial x_j} \left(\Gamma_k \frac{\partial k}{\partial x_j} \right) + G_k - Y_k \quad (18)$$

$$\frac{\partial}{\partial t}(\rho \omega) + \frac{\partial}{\partial x_i}(\rho u_i \omega) = \frac{\partial}{\partial x_j} \left(\Gamma_\omega \frac{\partial \omega}{\partial x_j} \right) + G_\omega - Y_\omega + D_\omega \quad (19)$$

where G represents generation of turbulent kinetic energy, k, or specific dissipation rate, ω, Y represents dissipation of k or ω, D_ω represents the cross-diffusion term, and Γ represents the effective diffusivity of k or ω. Further details regarding these equations are available in Ref. 9.

The turbulent viscosity for the k-ω SST model is evaluated using:

$$\mu_T = \rho\alpha \frac{k}{max(\alpha\omega, F_2 S)} \tag{20}$$

with coefficients $\alpha = 5/9$, $F_2 = tanh\left(\Phi^2\right)$, and

$$\Phi = max\left[2\frac{\sqrt{k}}{0.09\omega y}, \frac{500\mu}{\rho y^2 \omega}\right] \tag{21}$$

where y is distance from the nearest wall. The eddy viscosity can be rewritten as

$$\mu_T = \frac{C_\mu^{SST}}{\beta^*}\frac{\rho k}{\omega} \tag{22}$$

where

$$C_\mu^{SST} = 0.09 \times \frac{\alpha}{max(\alpha, F_2 S)}. \tag{23}$$

The motivation to include a new scalar modeling variable comes from our previous work on rotation/curvature sensitive EVMs [10], in which we found that the direct implementation of a rotation/curvature sensitized eddy viscosity coefficient introduced instability in some test cases, and spatial filtering introduced for stability purposes significantly increased the computational cost. As an alternative, the current model includes a structure variable related to a fluctuating transverse velocity component. As such, the new approach borrows from the k-ε-υ^2 framework originally proposed by Durbin [11]. Herein, the transport equation for the new scalar variable υ^2 is based on the conceptual description:

$$\frac{D\upsilon^2}{Dt} = \frac{D}{Dt}\left(\frac{\upsilon^2}{k}k\right) = \frac{\upsilon^2}{k}\frac{Dk}{Dt} + k\frac{D}{Dt}\left(\frac{\upsilon^2}{k}\right) \tag{24}$$

The second term on the right hand side of equation (24) is intended to represent the changes in turbulence structure due to system rotation and curvature effects. The eddy viscosity is redefined in terms of the new scalar variable:

$$\mu_T = \frac{C_\mu^{SST}}{\beta^*}\frac{\rho\sqrt{k}\sqrt{\upsilon^2}}{\omega} \tag{25}$$

.

The RC effect enters the model via υ^2. Under the condition of weak equilibrium, the new scalar υ^2 approaches the turbulence kinetic energy k such that

$$\upsilon^2 = \left(\frac{C_\mu^{rot}}{C_\mu^{non-rot}}\right)^2 k = \eta^2 k \tag{26}$$

where C_μ is rotation-sensitive eddy viscosity coefficient similar to that derived by York et al. [2], the superscript ***rot*** stands for rotating systems and ***non-rot*** stands for non-rotating systems. Considering the model form used by York et al. [2], the transport equations for turbulent kinetic energy k and dissipation rate ε in homogeneous shear flow can be cast as:

$$\frac{dk}{dt} = P - \varepsilon, \tag{27a}$$

$$\frac{d\varepsilon}{dt} = C_{\varepsilon 1}\frac{\varepsilon}{k}P - C_{\varepsilon 2}\frac{\varepsilon^2}{k} \tag{27b}$$

$$\frac{d}{dt}(\varepsilon/k) = (C_{\varepsilon 1} - 1)\frac{\varepsilon}{k^2}P - (C_{\varepsilon 2} - 1)\frac{\varepsilon^2}{k} \tag{27c}$$

Under weak equilibrium, with constants $C_{\varepsilon 1} = 1.44$, $C_{\varepsilon 2} = 1.92$:

$$(P/\varepsilon)_\infty = C_\mu\left(\frac{Sk}{\varepsilon}\right)_\infty^2 = (C_{\varepsilon 2-1})/(C_{\varepsilon 1} - 1) = 2.09 \tag{28}$$

$$\left(\frac{Sk}{\varepsilon}\right)_\infty = \left(\frac{2.09}{C_\mu}\right)^{1/2}. \tag{29}$$

Equation (29) along with York et al. eddy viscosity coefficient expression (Eq. 11) is solved for the weak equilibrium values of C_μ for different (ω_m/S) values. A functional relationship for the ratio of rotating and non-rotating eddy viscosity coefficient with (ω_m/S) is then developed. Figure 1 shows the resulting variation of $\eta = \left(\frac{C_\mu^{rot}}{C_\mu^{non-rot}}\right)$ with frame rotation rate (ω_m/S). The formulation in Eq. (11) captures the flow instability in the range of $0 \le \omega_m / S \le 0.25$ with maximum growth rate at $\omega_m / S = 0.23$. Although most flows of engineering interest occur in this range, we extended our model's range to $0.0 \le \omega_m / S \le 0.5$. This extension is based on the symmetric bifurcation diagram for rotating shear flow using the weak equilibrium analysis of the Speziale, Sarkar, and Gatski differential Reynolds stress model [12]. An explicit expression developed for the functional relationship between η and ω_m/S is a fifth order polynomial:

$$\eta(x) = a_5 x^5 - a_4 x^4 + a_3 x^3 - a_2 x^2 + a_1 x + a_0 \tag{30}$$

with $x = (\omega_m/S)$, and model coefficients:

$$a_0 = 1.0 \qquad a_3 = 331.5$$
$$a_1 = 18.57 \qquad a_4 = 437.8 \qquad (31)$$
$$a_2 = 112 \qquad a_5 = 145.7$$

When the value of (ω_m/S) goes outside the working range of this formulation, η is set to zero, which has the effect of relaminarizing the flow under the condition of stabilizing curvature.

For the structural source term of the new scalar transport equation (Eq. 24), an assumption analogous to linear return to isotropy of the Reynolds stress tensor is made in such a way that the model will return back to the SST k-ω model in regions where the curvature and rotation effect in the flow is negligible. The following expression carries the structural information:

$$C_R \beta^* \omega \left(\eta^2 k - \upsilon^2\right) \qquad (32)$$

$$C_{\upsilon^2} = C_R \beta^* = 0.162 \qquad (33)$$

$$\psi = C_{\upsilon^2} \omega . \qquad (34)$$

where $C_R = 1.8$, is from Rotta's return-to-isotropy model [13] and $\beta^* = 0.09$ comes from the SST k-ω model. The model transport equation for υ^2 is therefore:

$$\frac{D\rho\upsilon^2}{Dt} = \frac{\upsilon^2}{k} P - \beta^* \rho \upsilon^2 \omega + \rho\psi(\eta^2 k - \upsilon^2) + \frac{\partial}{\partial x_j}\left(\Gamma_k \frac{\partial \upsilon^2}{\partial x_j}\right). \qquad (35)$$

The scalar υ^2 becomes identical to turbulent kinetic energy k, in the regions where curvature and rotational effects are negligible and the model returns SST k-ω results.

MODEL VALIDATION

The new variant of the SST k-omega model was implemented into the commercial flow solver FLUENT® 6.2.16. A pressure based segregated solver with SIMPLE pressure velocity coupling scheme was used for all test cases. Second order upwind discretization was used for all the convective variables. For the convergence evaluation and comparison purposes, a fully developed U bend test case was run in an identical environment using both SST k-ω and the new variant of SST k-ω model. The new model requires approximately 17% more computation time per iteration, which is expected given the fact that it has one additional transport equation to solve. The convergence rate of new model compared to the SST k-ω was very much case dependent. It appears that the new scalar υ^2, in some test cases (for example U bend, Hump model) reaches an equilibrium solution faster than the turbulent kinetic energy k and drives the solution towards convergence faster than the standard SST k-ω model.

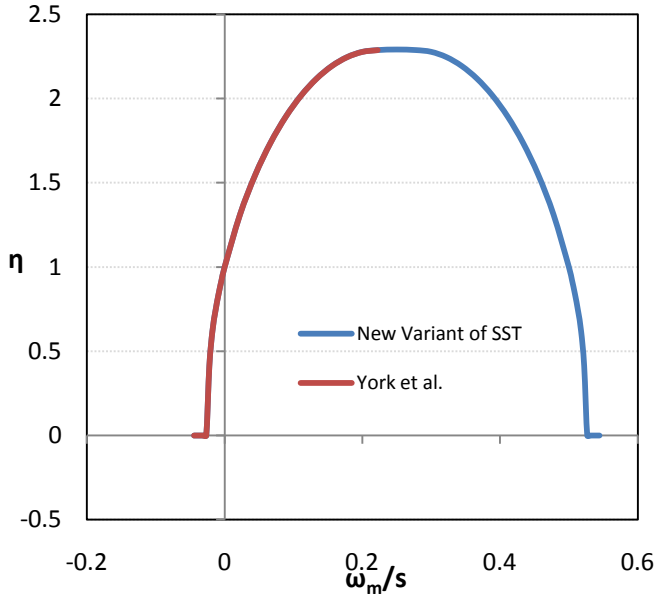

Fig 1. Bifurcation diagram for the new variant of SST k-ω model.

Homogeneous Shear Flow

Homogeneous shear flow is widely used as a demonstration case for the study of effects of rotating reference frame on modeled turbulence production. Since the flow is homogeneous (i.e. no streamline curvature effects), the term ω_m appearing in the model equations is simply equal to the reference frame rotation rate and there is no convective or diffusive transport. For the cases shown here, given an applied strain rate S, the initial value of specific dissipation rate was $\omega_0 = 3.3S$, and the initial value of turbulent kinetic energy, k_0, was arbitrary. This matches the conditions used by Bardina et al. [12] for large-eddy simulations (LES) of this flow, the results of which were used for comparison purposes. The initial value of υ^2 was set equal to k_0, which is the equilibrium result for non-rotating flow.

Three different frame rotation rates were considered, corresponding to no rotation ($\omega_m/S = 0$), stabilizing rotation ($\omega_m/S = -0.5$), and destabilizing rotation ($\omega_m/S = 0.25$). Figure 2 shows the temporal evolution of turbulent kinetic energy for the non-rotating case, with dimensionless time denoted as $t^* = St$. The model variant results are in good agreement with the LES results of Bardina et al. [14] and are identical to the k-ω SST model. Figure 3 shows stabilizing rotation in which turbulent kinetic energy exhibits temporal decay, and the new model successfully captures this behavior. Figure 4 shows the destabilizing rotation case that results in a significant increase in the production of turbulent kinetic energy in comparision to the non-rotating case. Although an eddy-viscosity model is unable to reproduce the initial decay, the new model does show a significant enhancement of turbulent production, similar to the LES results.

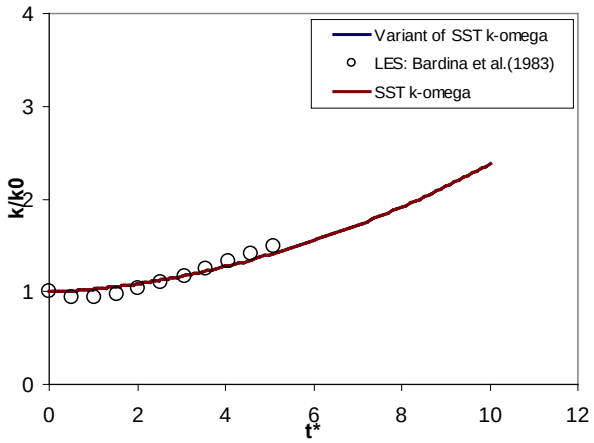

Fig 2. Temporal growth of turbulent kinetic energy for non-rotating homogeneous turbulence in plane shear, $\omega_m/S = 0$.

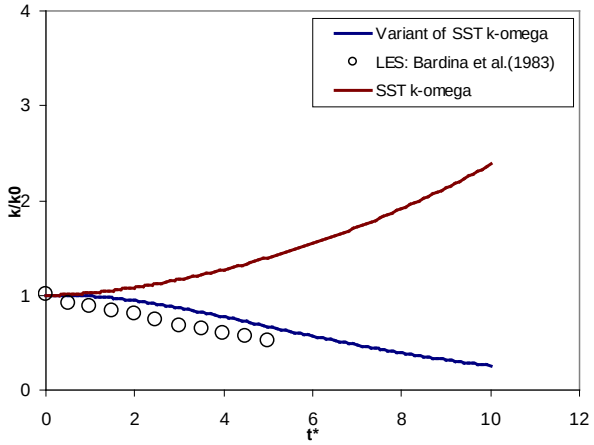

Fig 3. Temporal decay of turbulent kinetic energy for homogeneous turbulence in plane shear with stabilizing rotation, $\omega_m/S = -0.5$.

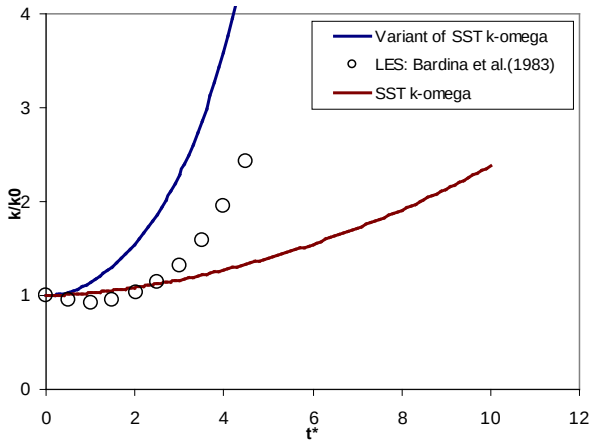

Fig 4. Temporal growth of turbulent kinetic energy for homogeneous turbulence in plane shear with destabilizing rotation, $\omega_m/S = 0.25$.

Rotating Channel Flow

Figure 5 shows a schematic of rotating two-dimensional channel flow. For the test cases here, Reynolds number based on friction velocity and channel half-height, Re_τ = 194, was chosen to match the DNS data of Kristoffersen and Andersson [15]. Simulations were carried out for rotation numbers Ro = 0, 0.05 and 0.5, where Ro = $\frac{\omega_m H}{U_m}$, and U_m is the average velocity through the channel. A Cartesian grid of size 10x200 (streamwise x wall-normal) was used to simulate the fully developed turbulent rotating channel flow with periodic boundary conditions applied in the streamwise direction. The maximum wall y^+ value for the channel was 0.14. Results are presented in terms of the mean velocity and turbulent kinetic energy profiles, with velocity magnitude normalized using the average channel velocity and turbulent kinetic energy normalized by the square of the average wall friction velocity.

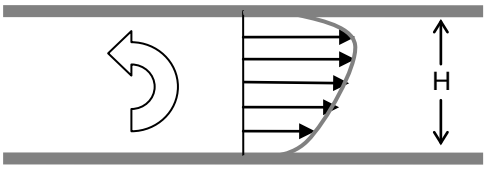

Fig 5. Schematic diagram of fully developed rotating channel flow with channel height H.

Figure 6 shows the velocity profile for the non-rotating channel. Both models produce results that closely match the reference DNS data, and produce results identical to one another.

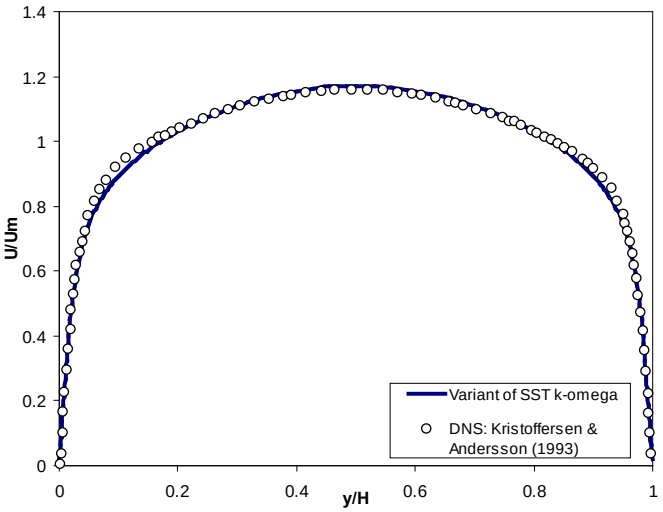

Fig 6. Velocity profile for non-rotating channel flow.

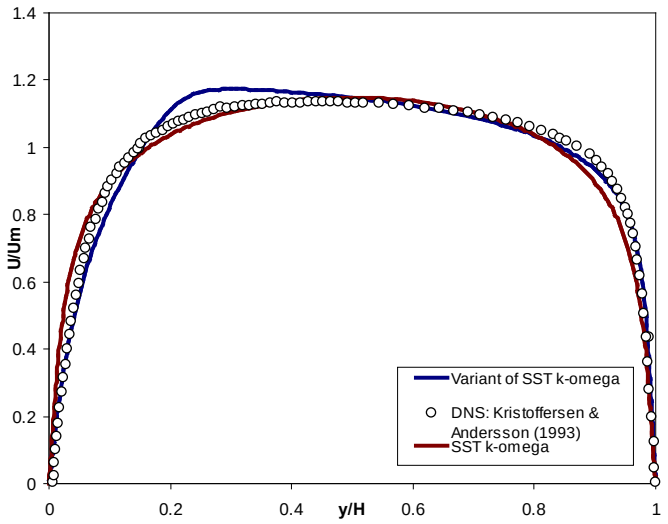

Fig 7. Velocity profile for rotating channel flow, Ro =0.05

In Figures 7 and 8 at rotation numbers Ro = 0.05, 0.5, the new variant of the k-ω SST model captures the asymmetric velocity distribution indicated by the DNS data. The SST model, not being sensitized to system rotation, doesn't respond to rotational effects. Figures 9 and 10 show the turbulent kinetic energy profiles for the respective rotation numbers, and the new variant of the SST model responds to the imposed rotation close to the DNS results. Note that the new model indicates suppression of turbulent kinetic energy on the stabilizing side of the channel, and augmentation on the destabilizing side, in agreement with the DNS results and with previous experiments reported in the literature.

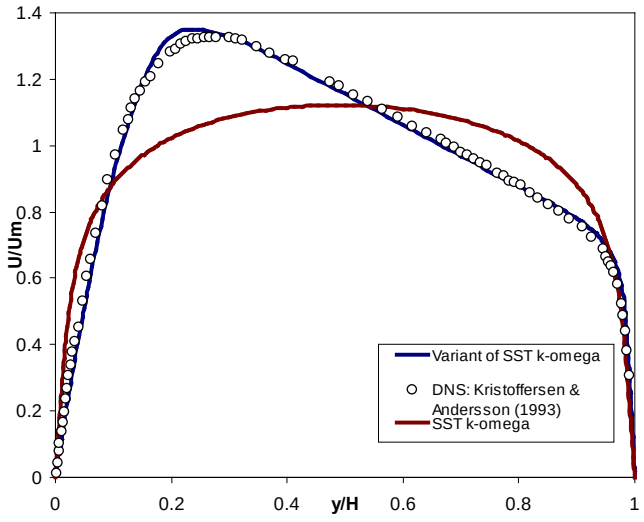

Fig 8. Velocity profile for rotating channel flow, Ro = 0.5

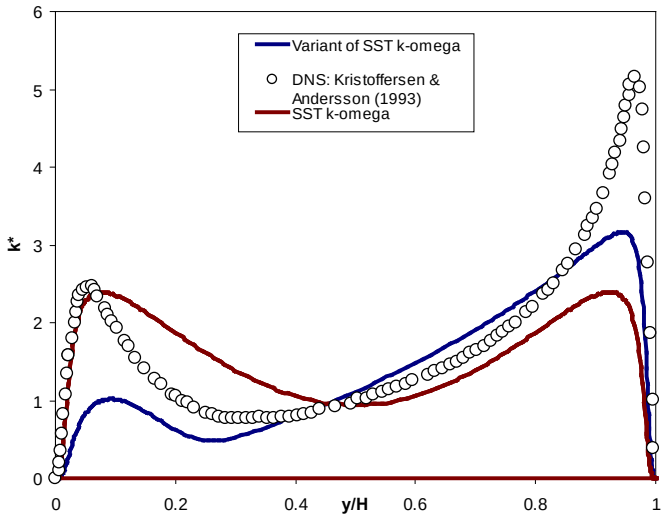

Fig 9. Turbulent kinetic energy profile for channel flow rotating at Ro = 0.05.

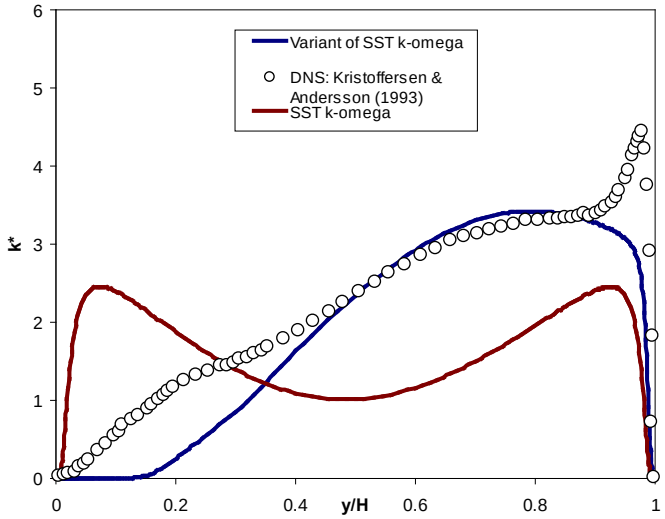

Fig 10. Turbulent kinetic energy profile for rotating channel flow Ro = 0.5

U-Bend flow

U-bend flows are commonly used to test turbulence model performance for cases with strong streamline curvature effects followed by a flow separation. A computational domain based on the two-dimensional U-Duct experiment performed by Monson et al. [16] as shown in Fig. 11 was used for this test case. The Reynolds number based on average velocity and channel height was $Re_H = 10^6$. A Cartesian grid 440x94 (streamwise x wall-normal) cells with a maximum wall y^+ value of 0.47 was used for the simulations. The inlet conditions, including velocity profile, turbulent kinetic energy profile and

specific dissipation rate profile were specified at the inlet to match the experimental values reported in Ref. 16. Results were compared to measured data at locations 90° and 180° through the bend, as indicated in Fig. 11, in terms of velocity and turbulent kinetic energy profiles. The mean velocity was normalized using average velocity in the channel, U_m, and the turbulent kinetic energy was normalized by $U_m^2/1000$.

Figure 12 shows the mean velocity profile at the 90° location. The new variant of the k-ω SST model successfully captures the velocity profile at the concave outer surface of the duct where turbulence augmentation occurs. In contrast, the standard k-ω SST model underpredicts the velocity magnitude in this region, similar to other results in the literature using eddy viscosity models (c.f. York et al. [2]). Figure 13 shows the turbulent kinetic energy profile at the 90° location. The new model predicts turbulence augmentation near the concave wall and turbulence suppression near the convex wall, while the standard model shows less sensitivity towards the streamline curvature effect. In terms of RC effects, the new model results are in better agreement with the experimental data.

Figures 14 and 15 show the velocity and turbulent kinetic energy profiles at the $\theta = 180°$ location. The new variant successfully captures the characteristic profiles of velocity and turbulent kinetic energy on the outer wall of the duct. The experimental data shows a separation bubble at the inner wall at $\theta = 180°$ and a sudden increase in turbulent kinetic energy. Both models successfully capture the separation bubble and turbulence peak but fail to predict the correct turbulence spike and separation length. As pointed out in previous studies [17-19], the separation and reattachment regions are typically not well captured by RANS models. It is likely that a hybrid RANS-LES approach would perform better in this region.

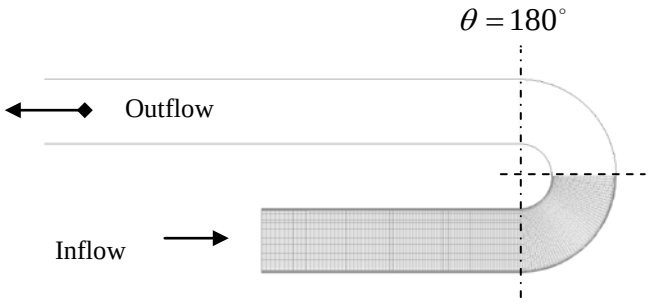

Fig 11. Computational domain and mesh for 2-D U-bend test case.

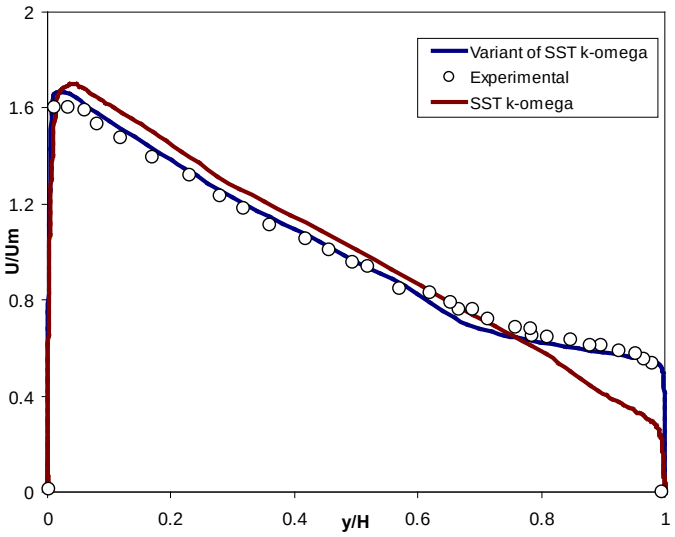

Fig 12. Velocity profile at $\theta = 90^\circ$ in the U-bend

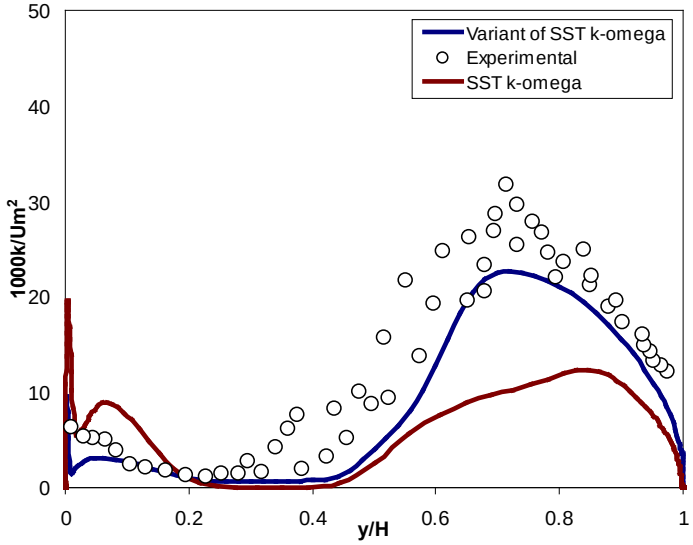

Fig 13. Turbulent kinetic energy profile at $\theta = 90^\circ$ in the U-bend.

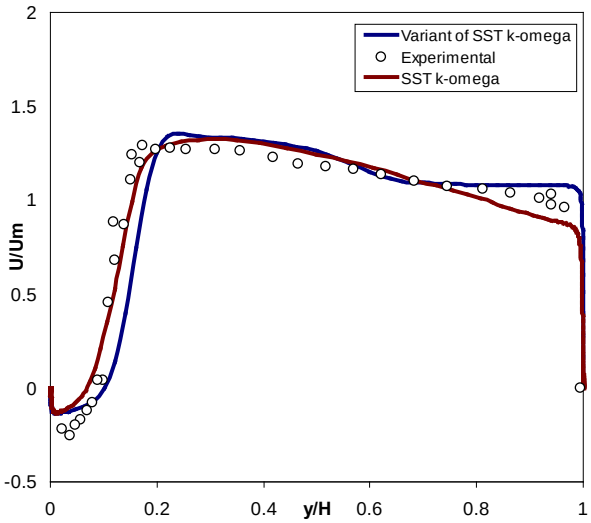

Fig 14. Velocity profile at $\theta = 180°$ in the U-bend.

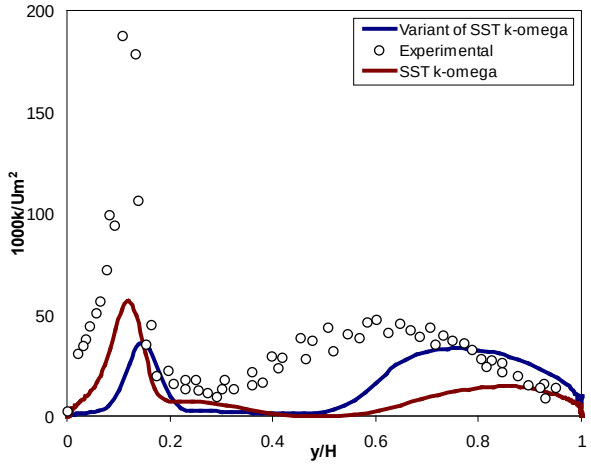

Fig 15. Turbulent kinetic energy plot at $\theta = 180°$ in the U-bend.

Flow over Hump Model

The hump model is an interesting test case of flow control application for steady and unsteady RANS models. It has a wall mounted Glauert-Goldschmied (having convex curvature over the front part and concave curvature over the rear part) type body. The body has a chord length *c* of 0.42 m and height of *h* = 0.0538 m. For the flow control, a slot is located at 0.65*c* as shown in Figure 16. The slot has a span of 0.5842 m and the suction rate is 0.01518 kg/s for the test case considered. Pressure at the suction slot was adjusted to achieve the desired mass flux. Reynolds number based on the chord length for this case is 936,000. The first cell-wall distance was carefully chosen to maintain wall y^+ value within 1. A 2D structured 240x560 medium grid was generated for testing purposes as shown in Figure 17. Details of the experiment are available in Refs [20-22]. For the present model comparison, pressure coefficient and turbulent shear stress profiles were examined at certain locations of the hump. A two times refined grid in both directions was generated to study the grid convergence and grid refinement effect on the new model. Figure 18 shows the pressure coefficient plot for the medium and fine mesh using the new variant of the SST k-ω model. Results are almost identical for both mesh sizes. There was a minimal mean flow modification due to grid refinement. Other results presented here are based on the medium grid. Figure 19 shows the pressure coefficient profile on the hump surface. Both the SST and the new variant of SST produced almost identical results. Both models overpredicted the length of the separation bubble. These results are almost identical with the results reported by Rumsey and Swanson [22] for the SST model. Rumsey and Swanson's result shows that the RANS based turbulence models, including some NLEVMs, tend to predict a large separation bubble. The new model slightly improved the turbulent stress at the location *x/c* = 0.8 compared to the SST model as shown in Figure 20. Similar to the U-Bend case above, it is surmised that substantial improvement in prediction of the separated flow region may require the use of a hybrid RANS-LES approach.

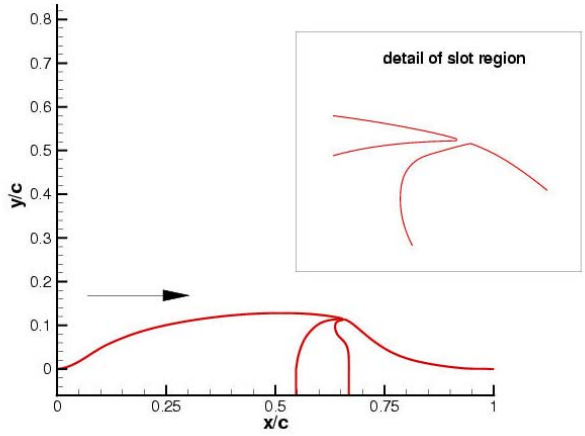

Fig 16. Schematic of Hump model

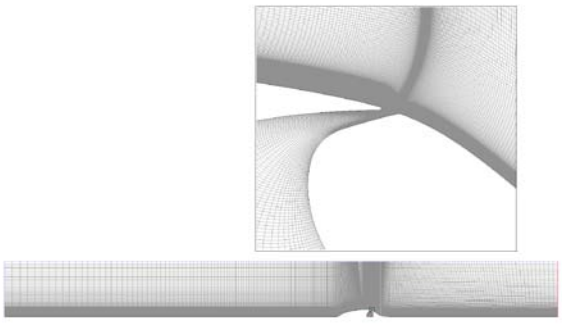

Fig 17. Hump grid used for steady suction flow control simulation. Expanded view of the mesh close to the suction slot region.

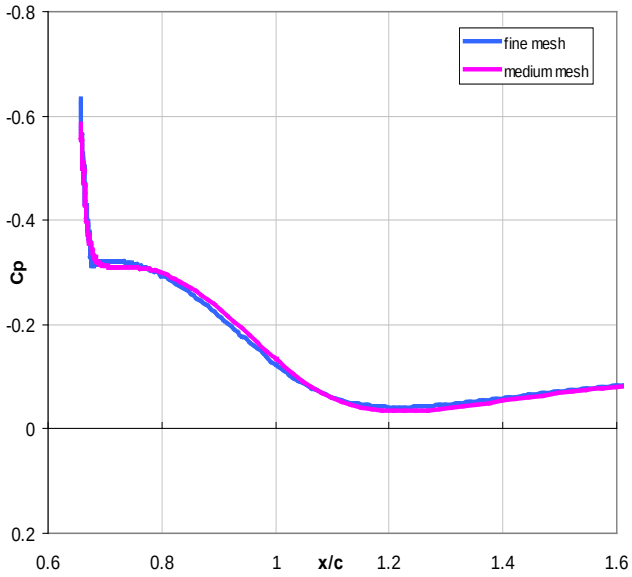

Fig 18. Effect of grid refinement on new variant of SST k-ω model.

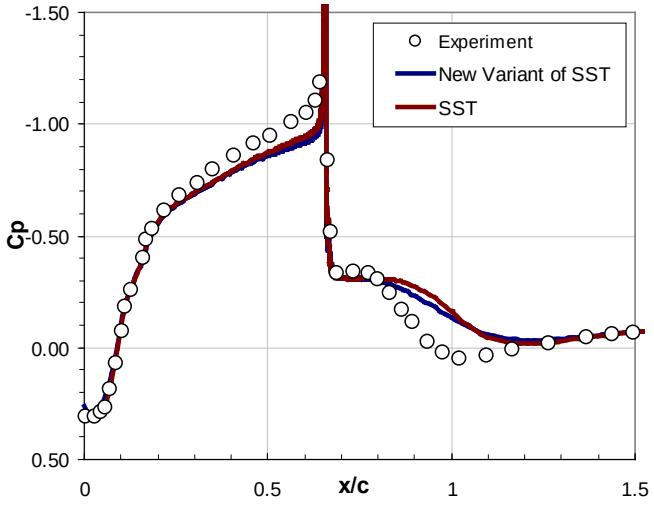

Fig 19. Pressure coefficient profile of hump model flow with steady suction control using SST model, and curvature and/or rotation sensitive new variant of SST.

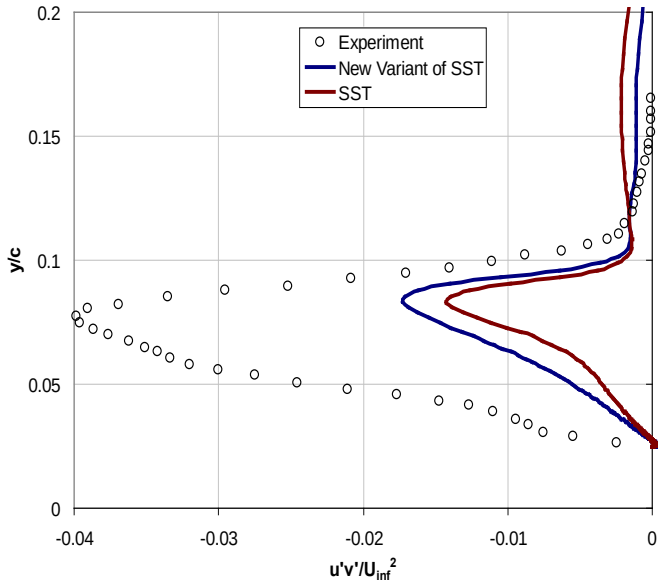

Fig 20. Turbulent shear stress profiles at x/c = 0.8.

CONCLUSION

A modified version of the SST k-ω model capable of accounting for rotation/curvature effects has been developed and presented. A new transport equation was introduced to capture the rotation/curvature effects along with the turbulent kinetic energy and specific dissipation rate equations. The reference frame rotation rate and streamline curvature effect enters through the v^2 transport equation, which in turn, enters the model via a modified expression for eddy-viscosity. The added scalar equation increased the computation time per iteration by almost 17%, but reduced the number of iterations required to get a converged solution, at least for the cases considered here. A number of test cases were run to evaluate the performance of the model focusing on rotating reference frames and streamline curvature, and the results showed improved agreement with the experimental and/or DNS data, in comparison to the standard k-ω SST model. The new model showed a good agreement with the LES data in rotating homogeneous shear flow case. The new model successfully captured the effect of system rotation in the rotating channel flow case. In the fully developed U-bend flow case, the model successfully captured the turbulent kinetic energy suppression in the convex wall and augmentation in the concave wall. Both SST and the new variant of SST fail to correctly capture the sudden turbulence spike at $\theta = 180°$ near the convex wall and the separation length. As for the hump model case, although the new model captured the turbulent kinetic energy augmentation due to concave curvature, it had the same deficiency in the separation region which happens to be an issue with EVMs. In contrast to prior efforts to include RC effects into the k-ω SST model [10], stability was not an issue for the present model in the test cases discussed here.

REFERENCES

[1] Gatski, T.B. and Speziale, C.G., "On Explicit Algebraic Stress Models for Complex Turbulent Flows", Journal of Fluid Mechanics", v. 254, 1993, pp. 59-78.

[2] York, W.D., Walters, D.K., and Leylek, J.H., "A Simple and Robust Linear Eddy-Viscosity Formulation for Curved and Rotating Flows", International Journal for Numerical Methods in Heat and Fluid Flow, in press.

[3] Girimaji, S.S., "A Galilean Invariant Explicit Algebraic Reynolds Stress Model for Turbulent Curved Flows," Physics of Fluids, v. 9, 1997, pp. 1067-1077.

[4] Wallin, S. and Johansson, A.V., "Modelling Streamline Curvature Effects in Explicit Algebraic Reynolds Stress Turbulence Models", International Journal of Heat and Fluid Flow, v. 23, 2002, pp. 721-730.

[5] Gatski, T.B. and Jongen, T., "Nonlinear Eddy Viscosity and Algebraic Stress Models for Solving Complex Turbulent Flows," Progress in Aerospace Sciences, v. 36, No. 8, 2000, pp. 655-682.

[6] Wang, X. and Thangam, S., "Developemnt and Application of an Anisotropic Two-Equation Model for Flows with Swirl and Curvature", ASME Journal of Applied Mechanics, v. 73, 2006, pp. 397-404.

[7] Rumsey, L. and Gatski, T.B., "Isolating Curvature Effects in Computing Wall Bounded Turbulent Flows", AIAA paper No. 2001-0725.

[8] Spalart, P.R., and Shur, M.L., "On the Sensitization of Turbulence Models to Rotation and Curvature", Aerospace Science and Technology, v. 1, No. 5, 1997, pp. 297-302.

[9] Menter, F. R., "Improved Two-Equation K-omega Turbulence Models for Aerodynamic Flows", NASA Technical Memorandum 103975, 1992.

[10] Dhakal, T. P., Walters, D. K., "Curvature and Rotation Sensitive Variants of the K-Omega SST Turbulence Model", Proceedings of ASME 2009 Fluids Engineering Division Summer Meeting, paper No. 78397.

[11] Durbin, P.A., "Near-Wall Turbulence Closure Modeling without Damping Functions," Theoretical and Computational Fluid Dynamics, v. 3, 1991, pp. 1-13.

[12] Speziale, C.G., Sarkar, S., and Gatski, T.B., "Modelling the Pressure-Strain Correlation of Turbulence: An Invariant Dynamical Systems Approach," Journal of Fluid Mechanics, v. 227, 1991, pp. 245-272.

[13] Rotta, J.C., "Recent Attempts to Develop a Generally Applicable Calculation Method for Turbulent Shear Flow Layers," AGARD Turbulent Shear Flows, v. 11, 1972, pp. 11-12.

[14] Bardina, J., Ferziger, J.H., and Reynolds, W.C., "Improved Turbulence Models Based on Large-eddy Simulation of Homogeneous, Incompressible Turbulent Flows", Stanford University Technical Report, TF-19, 1983.

[15] Kristoffersen, R. and Andersson, H.I., "Direct Numerical Simulation of Low Reynolds-Number Turbulent Flow in a Rotating Channel", Journal of Fluid Mechanics, v. 256, pp. 163-197.

[16] Monson, D.J., Seegmiller, H.L., McConnaughey, P.K., and Chen, Y.S., "Comparison of Experiment with Calculations Using Curvature-Corrected Zero and Two Equation Turbulence Models for a Two-Dimensional U-Duct", AIAA Paper No. 90-1484.

[17] Spalart, P. R. "RANS Modelling into a Second Century", International Journal of Computational Fluid Dynamics, Editorial, Vol.23, No. 4, 2009, pp. 291-293.

[18] Hirsch, C. and Tartinville, B., "Reynolds-Averaged Navier-Stokes Modelling for Industrial Applications and Some Challenging Issues", International Journal of Computational Fluid Dynamics, Vol.23, No. 4, 2009, pp. 295-303.

[19] Smirnov, P. E. and Menter, F. R., "Sensitization of the SST Turbulence Model to Rotation and Curvature by Applying the Spalart-Shur Correction Term", Journal of Turbomachinery, Vol. 131, 2009, No. 041010.

[20] Greenblatt, D., Paschal, K. B., Yao, C.-S., Harris, J., Schaeffler, N. W., Washburn, A. E., "A Separation Control CFD Validation Test Case, Part 1: Baseline and Steady Suction," AIAA Journal, Vol 44, No. 12, 2006, pp. 2820-2830.

[21] Rumsey, C. L., et al., "Summary of the 2004 Computational Fluid Dynamics Validation Workshop on Synthetic Jets", AIAA Journal, Vol 44, No. 2, 2006, pp. 194-207.

[22] Rumsey, C. L., and Swanson, R. C., "Turbulence Modelling for Active Flow Control", International Journal of Computational Fluid Dynamics, Vol. 23, No. 4, 2009, pp. 317-326.